Erzinger, J., Becker, K., Dick, H.J.B., and Stokking, L.B. (Eds.), 1995
Proceedings of the Ocean Drilling Program, Scientific Results, Vol. 137/140

6. PRIMARY AND SECONDARY VARIATIONS IN MAJOR AND TRACE ELEMENT GEOCHEMISTRY OF THE LOWER SHEETED DIKE COMPLEX: HOLE 504B, LEG 140[1]

Evelyn Zuleger,[2] Jeffrey C. Alt,[3] and Jorg Erzinger[2]

ABSTRACT

Rocks of the lower sheeted dike complex of Hole 504B sampled during Leg 140 were analyzed for major and trace element compositions to investigate the effects of igneous processes and hydrothermal alteration on the compositions of the rocks. The rocks are relatively uniform in composition and similar to the shallower dikes. They are moderately evolved mid-ocean-ridge basalts (MORB) with relatively high MgO (7.9–10 wt%) and Mg# (0.60–0.70), and have unusually low incompatible element contents (TiO_2 = 0.42–1.1 wt%, Zr = 23–62 ppm). Discrete compositional intervals in the hole reflect varying degrees of differentiation, and olivine and plagioclase accumulation in the rocks, and may be related to injection of packets of dikes having similar compositions. Systematic depletions of total REE, Zr, Y, TiO_2, and P_2O_5 in centimeter-size patches are most likely attributed to exclusion of highly differentiated, late-stage interstitial liquids from small portions of the rocks.

The rocks exhibit increased H_2O^+ reflecting hydrothermal alteration. Replacement of primary plagioclase by albite and oligoclase led to local gains of Na_2O, losses of CaO, and slightly positive Eu anomalies. Some mobility of P_2O_5 led to minor increases and decreases in P_2O_5 contents, and some local mobility of Ti may have occurred during alteration of titanomagnetite to titanite. Higher temperatures of alteration in the lower sheeted dikes led to breakdown of pyroxene and sulfide minerals and losses of Zn, Cu, and S to hydrothermal fluids. Later addition of anhydrite to the rocks in microfractures and replacing plagioclase caused local increases in sulfur contents. The lower sheeted dikes are a major source of metals to hydrothermal fluids for the formation of metal sulfide deposits on and within the seafloor.

INTRODUCTION

Understanding the structure, tectonics, petrology, and chemical alteration processes in the oceanic crust are among the most important goals of the Ocean Drilling Program (ODP). Our knowledge of the nature of oceanic basement is mainly drawn from studies of ophiolite complexes, remote geophysical surveys, and studies made on dredged or cored samples from the ocean floor. A generally layered model of the ocean crust has been proposed based on these studies (e.g., Raitt, 1963; Fox and Stroup, 1981). In this layered model, pelagic sediments (seismic Layer 1) cover a volcanic sequence of pillowed and massive basalts and breccias (Layer 2A and 2B). This upper section grades downward into a sheeted diabasic dike complex (Layer 2C), which is underlain by a plutonic sequence of gabbros and ultramafic cumulates (Layer 3). The volcanic section is generally altered at low temperatures up to greenschist conditions, and the underlying sheeted dikes are altered under greenschist grading downward to amphibolite facies conditions in the uppermost gabbros.

The only oceanic drill hole that clearly penetrates through the lavas of Layers 2A and 2B into the sheeted dike complex of Layer 2C is Deep Sea Drilling Project (DSDP)/ODP Hole 504B. Late in 1991, ODP Leg 140 returned to Hole 504B and drilled the hole 379 m deeper into the sheeted dike complex to a total depth of 2000.4 meters below seafloor (mbsf) (Figs. 1 and 2). This chapter presents the chemical compositions of the basement rocks from Hole 504B recovered during Leg 140, and discusses some of the processes responsible for the variations in their compositions.

SITE 504

Hole 504B is located in 5.9-m.y.-old crust, 201 km south of the intermediate spreading-rate Costa Rica Rift (Fig. 1; 1°13.611′N, 83°43.818′W; water depth 3460 m). Hole 504B is the deepest hole drilled into oceanic basement, penetrating 274.5 m of sediments, a 571.5-m volcanic section, a 209-m transition zone (TZ), and extending 954.5 m into a sheeted dike complex (SDC) (Fig. 2). Changes in alteration mineralogy with depth in the dikes, the increasing average grain size downward, the absence of glassy chilled dike margins in the lower dikes, and seismic data all indicate that, after the drilling on Leg 140, the hole now penetrates the lowermost portion of the sheeted dike complex, close to the transition downward from dikes to gabbros (Shipboard Scientific Party, 1988; 1992).

The upper 300 m of the volcanic section suffered oxidative alteration at high seawater/rock ratios and low temperatures (<100°C). Nonoxidative alteration affected the lower volcanic section at low water/rock ratios and possibly somewhat higher temperatures (up to 150°C). Greenschist mineral assemblages abruptly appear at 898 mbsf, and are present to the bottom of the hole (Fig. 2) (Alt et al., 1986; Alt et al., 1989; Shipboard Scientific Party, 1992). Rocks recovered from Hole 504B on Leg 140 are generally similar to those in the immediately overlying dikes (Shipboard Scientific Party, 1992). The Leg 140 rocks are affected by a pervasive slight background alteration, and are generally 10%–20% recrystallized. Locally the rocks are more intensively recrystallized (up to 80%–100%) in centimeter-size alteration halos along chlorite and actinolite veins and in irregularly shaped "patches" up to several centimeters across. Increasing amounts of actinolite downward in the dikes, and the local presence of hornblende and secondary anorthite in the lower dikes, indicate higher temperatures of hydrothermal alteration in the lower dikes (Alt et al., this volume; Laverne et al., this volume).

The rocks recovered from Hole 504B prior to Leg 140 are variably plagioclase-olivine-clinopyroxene phyric, and commonly contain accessory Cr-spinel. With the exception of two more-enriched units, the rocks are uniform in composition, interpreted to reflect a near steady-state magma chamber (Natland et al., 1983). The rocks are characterized by an unusual depletion in incompatible elements (Ti, Nb, Zr,

[1] Erzinger, J., Becker, K., Dick, H.J.B., and Stokking, L.B. (Eds.), 1995. *Proc. ODP, Sci. Results,* 137/140: College Station, TX (Ocean Drilling Program).
[2] Institut für Geowissenschaften und Lithosphärenforschung, Universität Giessen, Senckenbergstrasse 3, 6300 Giessen, Federal Republic of Germany.
[3] Department of Geological Sciences, 1006 C.C. Little Building, University of Michigan, Ann Arbor, MI 48109-1063, U.S.A.

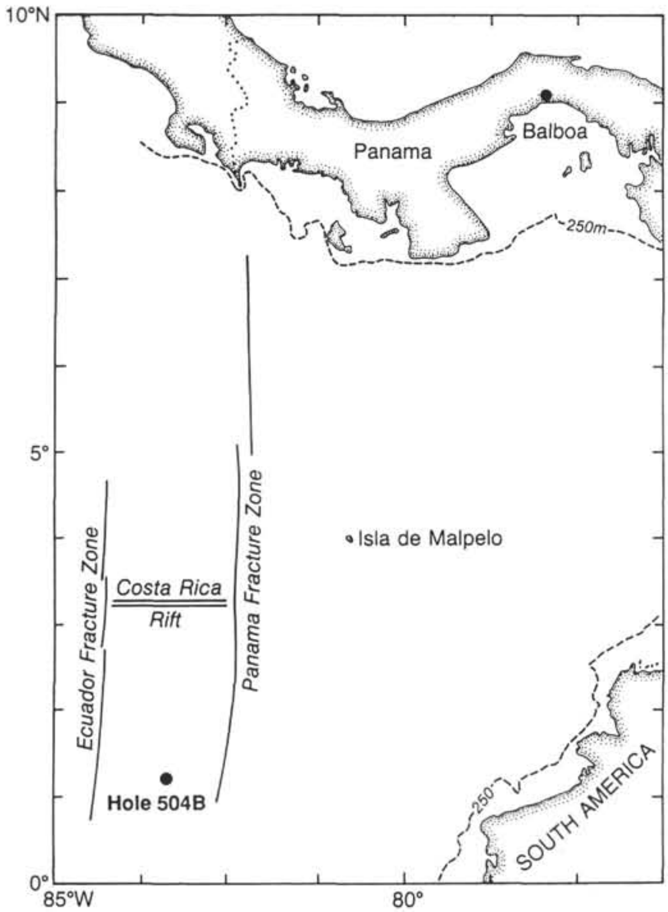

Figure 1. Location of DSDP/ODP Hole 504B south of the Costa Rica Rift in the eastern Pacific Ocean.

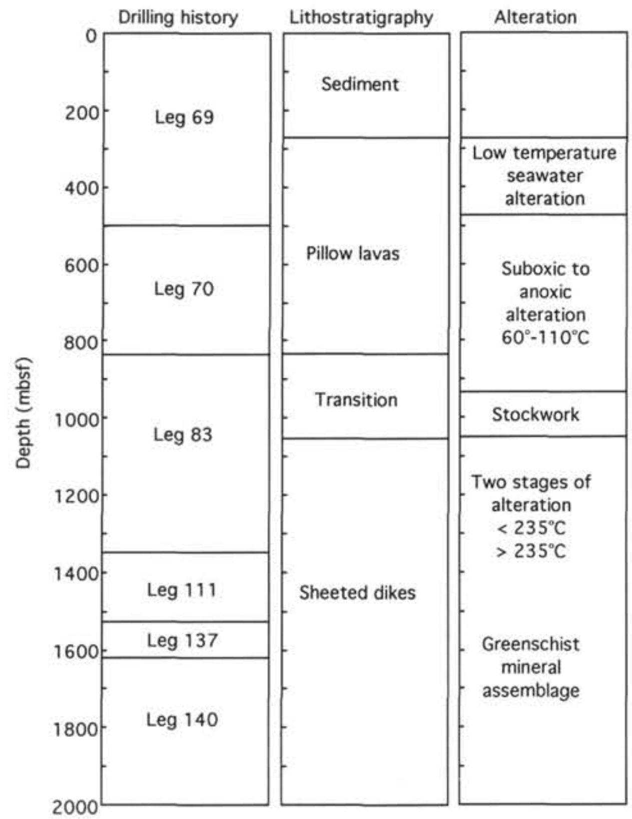

Figure 2. Lithostratigraphic and alteration summary, Hole 504B.

Y) and by incompatible element ratios similar to those of normal abyssal tholeiites (Autio and Rhodes, 1983; Emmermann, 1985; Hubberten et al., 1983).

MAJOR AND TRACE ELEMENT COMPOSITION

Analytical methods

This study is based on chemical data obtained for 85 whole rock samples, representing 62% of the 59 lithologic units recovered during Leg 140. Forty samples represent the freshest possible (i.e., the macroscopically least altered basalts, which are dark gray in color and have no visible veins or alteration discoloration). Any more intensively altered portions of the rocks or veins in the rocks were systematically removed by sawing prior to grinding for analysis. Throughout the following, these samples are referred to as "fresh rocks," and are listed as "D" (for dark gray) in Table 1. Another 16 samples exhibit a slightly lighter gray color and are affected by more intensive background alteration, and are listed as "L" (for light gray) in Table 1. Many of the latter are from fine-grained dike margins with abundant veins, and the more intensive alteration may actually represent coalescing of alteration halos around multiple veins. Twenty-three samples represent highly altered rocks, that is, light gray to greenish alteration halos along veins and alteration patches ("H" and "P," respectively, in Table 1). Six samples were cut so that both the intensively altered patch or halo and the immediately adjacent dark gray host rock could be analyzed and compared (labeled A and B in Table 1).

After the samples were washed with distilled water, dried, and crushed to <1 mm, they were powdered in an agate mill to a grain size <30 µm suitable for analysis. The following techniques were used.

1. The major element oxides (Si, Ti, Al, Fe, Mn, Mg, Ca, Na, P, K) were analyzed by X-ray fluorescence (XRF) on samples prepared as fused glass beads of lithium metaborate (rock to flux ratio 1:4) using a Phillips PW 1400 computerized spectrometer for intensity measurements and the alphas program to calculate concentrations.
2. Fe^{2+} was analyzed by manganometric titration.
3. H_2O^+ and CO_2 were measured on a Rosemount CWA 5003 analyzer.
4. S was determined on a Leco sulfur Sc 132 analyzer.
5. Measurements of Cr, Ni, Cu, Zn, Ga, Rb, Sr, Y, Zr, Nb, Pb, Th, and Ba were conducted by XRF on pressed powder pellets. The rhodium compton peak of the X-ray tube was used for matrix correction.
6. The rare earth elements (REE) were analyzed by optical emission spectroscopy (OES) using an inductively coupled plasma (ICP) for excitation. For this purpose the REE had to be quantitatively extracted by rock dissolution and concentrated using a chromatographic technique (Zuleger and Erzinger, 1988).
7. The mineral composition of selected samples was determined using a quantitative phase analysis procedure on a Siemens D 501 X-ray diffractometer (XRD) described by Emmermann and Lauterjung (1990). Only 31 samples could be analyzed by this method due to the small sample amounts remaining after chemical analysis.

Table 1 summarizes the chemical compositions of the 85 rock samples analyzed for this study, and Table 2 shows the REE data of selected samples. The values for K_2O (<0.05%), CO_2 (<0.1%), Rb, Pb, Th, Nb (<5 ppm), and Ba (<20 ppm) were found to be below the detection limit of the methods used, and are hence not reported. The precision of major and trace element determination was tested by duplicate measurements on selected samples. The accuracy was checked by carrying the international reference rock BHVO-1, and the Leg 140 interlaboratory standard Bas 140 (Sparks and Zuleger, this volume) as unknowns through the whole procedure. The chemical results are given in Table 3 along with the analytical errors and recommended concentration values (Govindaraju, 1989). The analytical accuracy of different methods is given in Table 4. Also given are Fe_2O_{3T} (total iron calculated as Fe_2O_3), FM-value ($[FeO_{total}/FeO_{total}+MgO] \cdot 100$), an oxidation index ("ox" expressed as $Fe_2O_3 \cdot 100/Fe_2O_{3T}$), and the Mg number (Mg# = MgO/MgO+FeO calculated 90% of total iron as FeO) (Table 1). The results of the quantitative phase analysis are given in Table 5. The analytical error of the determination is calculated with ±10%.

RESULTS AND DISCUSSION

Mineralogical Effects of Alteration

Of the 379 m drilled during Leg 140, 56.86 m of core was recovered, or about 13% of the drilled section. The rocks are aphyric to moderately phyric plagioclase-pyroxene-olivine diabases that are all mineralogically and chemically altered to some extent. The degree of alteration, defined as the abundance of secondary minerals, was visually estimated in thin section (Table 1). Alteration was also estimated in shipboard thin sections that were point counted for alteration phases to ascertain the reliability of the visual estimates. The visual estimates agree within 5%–10% of the estimates from shipboard point counts. Even the least altered dark gray samples are affected by a pervasive background alteration of about 10%–20%. The light gray rocks exhibiting more intensive background alteration are 20%–70% recrystallized. The light gray to greenish halos around veins and the alteration patches are generally more than 50% altered and range up to 90% altered.

Amphibole, chlorite, and albite are ubiquitous secondary minerals replacing primary minerals and interstitial material. The amphiboles are mainly actinolitic hornblende to magnesiohornblende, but also range to actinolite and local edenitic hornblende (Alt et al., this volume; Laverne et al., this volume). Actinolitic amphibole, plus fine-grained magnetite (a few microns), partly replaces clinopyroxene and interstitial material and is the most abundant alteration phase in all rocks. Olivine is commonly replaced by chlorite, chlorite + quartz, mixed-layer chlorite-smectite, actinolitic amphibole, or by talc and magnetite in some slightly altered samples. Plagioclase is partly replaced by albite, oligoclase, and minor laumontite, prehnite, and anhydrite in irregular patches and veins, and the outer rims of plagioclase in patches and halos are commonly replaced by secondary anorthite (Laverne et al., this volume). Titanite usually occurs as tiny crystals in interstitial areas or together with ilmenite replacing igneous titanomagnetite. The highly altered alteration patches often contain irregular amygdules, 0.01–10 mm across, that are filled with actinolite, chlorite, epidote, quartz, laumontite, and prehnite. Patches also contain greater amounts of prehnite and anhydrite than do the dark gray host rocks.

The quantitative analysis of mineral abundances in whole rocks by XRD shows that plagioclase and clinopyroxene contents decrease with increasing alteration, whereas the amphibole content increases (Fig. 3). In some samples talc and quartz were also detected. Figure 4 shows, in detail, that the dark gray host rocks contain higher contents of plagioclase and clinopyroxene than are in the associated alteration patch or halo portion. In comparison, the amphibole content, mainly actinolite, increases by a factor of two to three.

Veins are common throughout the core, and mainly consist of amphibole, chlorite, or a combination of these minerals. Later veins of epidote or epidote + quartz cut across the actinolite veins, and anhydrite and zeolites are interpreted to be the last alteration products (Shipboard Scientific Party, 1992). Local secondary clinopyroxene, plus hornblende and calcic secondary plagioclase, indicate early high-temperature (400°–500°C) hydrothermal alteration. This was followed by alteration at varying (lower) temperatures and fluid compositions, which produced the varying amphibole compositions and greenschist minerals, which are followed by zeolites and prehnite at the lowest temperatures (Laverne et al., this volume). The presence of talc replacing olivine, and relict olivine mark intervals where water/rock ratios were low and alteration effects are minimal (e.g., 1700–1750 mbsf; Shipboard Scientific Party, 1992).

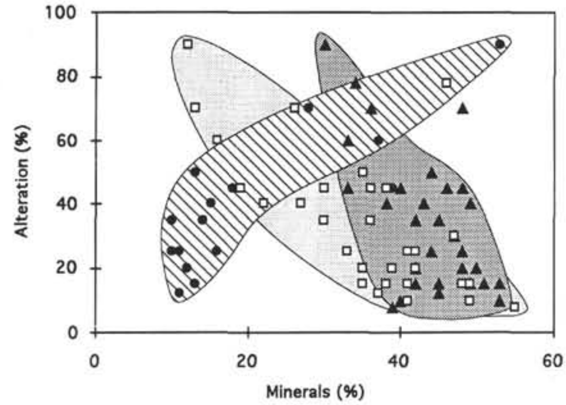

Figure 3. Degree of alteration vs. plagioclase, clinopyroxene, and amphibole content. Solid circles = amphibole; solid triangles = plagioclase; open squares = clinopyroxene.

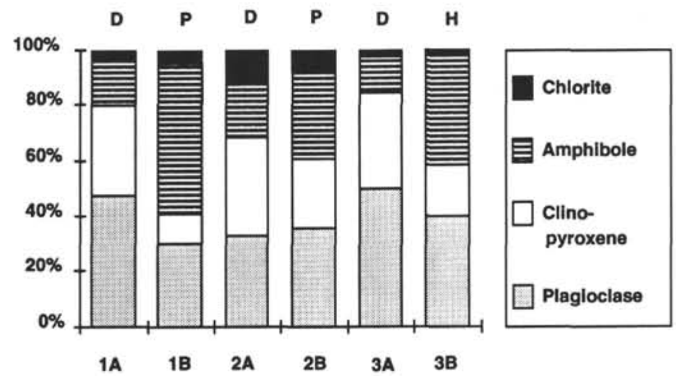

Figure 4. Mineral composition of three samples, separated in halo- (H) or patch- (P) rich parts and surrounding host rocks (D). Key to samples: 1A = 140-504B-187R-1, 59–63 cm A; 1B = 140-504B-187R-1, 59–63 cm B; 2A = 140-504B-222R-1, 115–120 cm A; 2B = 140-504B-222R-1, 115–120 cm B; 3A = 140-504B-235R-1, 21–24 cm A; 3B = 140-504B-235R-1, 21–24 cm B.

Primary Chemical Variations

In general the major element data of crustal rocks cored during Leg 140 exhibit a relatively uniform chemical composition, as seen in the previously drilled sections above 1621 mbsf (Emmermann, 1985; Hubberten et al., 1983). The samples studied in the present work represent moderately evolved mid-ocean-ridge basalts with relatively high MgO contents between 7.9 and 10 wt% and Mg numbers between 0.60 and 0.70. According to their normative mineralogy, the diabases are classified as olivine to slightly quartz normative tholeiites. However, the rocks are unusually low in incompatible elements (TiO_2 = 0.42–1.1 wt%, Zr = 23–62 ppm).

Despite the relative uniform composition of the rocks, some variations in the "fresh" rocks occur. Cr, Ni, Sr, and CaO/CaO + Na_2O are positively correlated with Mg number, whereas SiO_2, TiO_2, Y, and Zr exhibit negative correlations with Mg number, reflecting varying degrees of differentiation (Autio et al., 1989), and perhaps some accumulation of olivine and plagioclase in the rocks. Some significant variations in compositions of "fresh" rocks apparently occur over vertical intervals in the core. Mg numbers (and the corresponding elements and oxides above) are relatively high in the interval from 1704 to 1734 mbsf, at about 1925 mbsf, and possibly from 1790 to 1830 mbsf, whereas TiO_2, Zr, and Y are low in these zones (Fig. 5 and

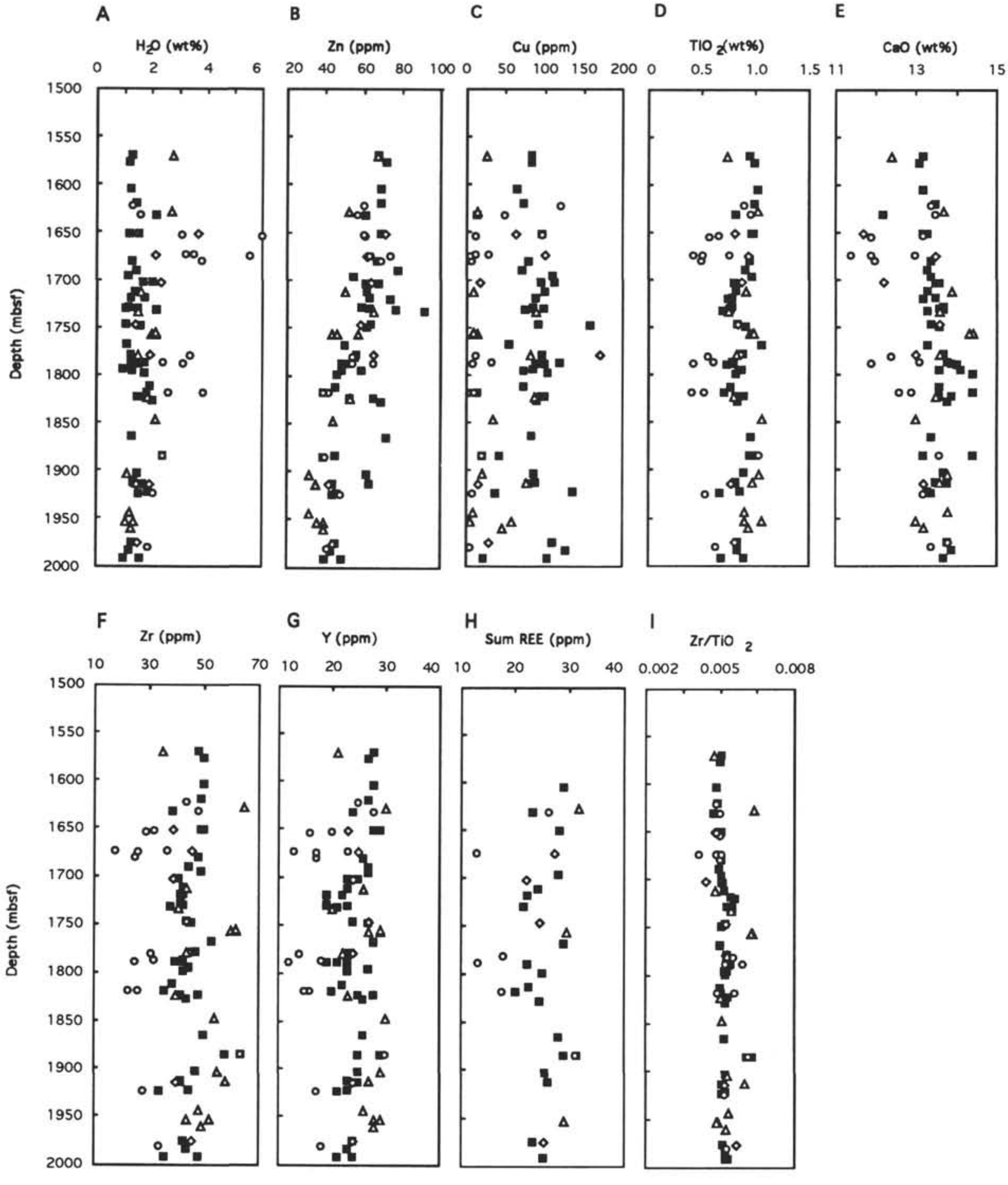

Figure 5. Downhole variations of Leg 140 diabases. Solid square = macroscopically dark, less altered diabases; open triangle = macroscopically light, high background alteration; open diamond = alteration halos around veins; open circle = green to gray alteration patches.

Table 1). Minima in Mg number (and corresponding elements and oxides) occur at 1850 and 1950 mbsf, coinciding with maxima in TiO_2, Zr, and Y contents. Because only 62% of the recovered units is represented by this data set, some of these variations could be attributed to a lack of sufficient data over certain intervals (e.g., at 1850 mbsf; Fig. 5). Combining the 79 shipboard chemical analyses to these plots adds to the scatter, but does not eliminate these general variations with depth. Such vertical variations may be related to intrusion of dikes in packets, whereby several dikes with similar compositions are intruded close together over a relatively short time span. Systematic intrusion of such packets would give rise to compositional variations on a scale larger than an individual dike, whereas intrusion of dikes from a different magma batch into a previous packet could give rise to scatter in such larger-scale variations.

The highly altered "patches" show obvious depletions in TiO_2, CaO, Y, Zr, and total REE values compared to less altered rocks (Fig. 5D–H), and are particularly noticeable in three different zones at 1650–1700 mbsf, 1780–1830 mbsf, and around 1920 mbsf (Fig. 5A). Despite depletion of the patches in TiO_2 and Zr, the patches have Zr/TiO_2 ratios identical to the mean value 0.0051 for the section, and

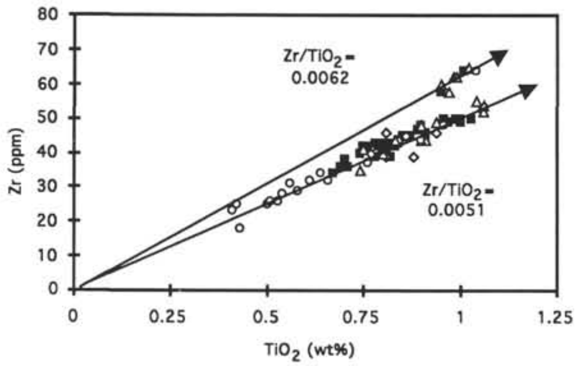

Figure 6. Zr vs. TiO_2 of Leg 140 diabases. Refer to Figure 5 for explanation of symbols.

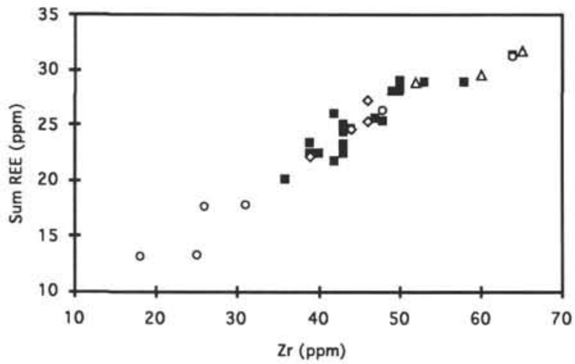

Figure 7. Total REE vs. Zr of selected Leg 140 diabases. Refer to Figure 5 for explanation of symbols.

it is only samples other than the patches that deviate significantly from the mean value of 0.0051 (Fig. 5I). Besides elevated Zr/TiO_2 (Fig. 6), the deviant samples are also enriched in Zr relative to total REE (Fig. 7), suggesting that they represent a second magmatic trend. Data for rocks recovered from all legs at Hole 504B show that the small group of samples with a Zr/TiO_2 ratio of 0.0062 fall within the range of the vast majority of rocks recovered from the rest of the hole (Fig. 8). Only a few units of enriched or transitional basalts with Zr/TiO_2 greater than 0.007 occur from sections drilled during Legs 70 and 83 sections (Autio and Rhodes, 1983; Emmermann, 1985).

The REE distribution patterns of Leg 140 whole rock samples (Fig. 9) are similar to those of samples from shallower in Hole 504B. Samples with varying percentages of alteration and alteration halos around veins generally show no significant differences from "fresh" rocks (Fig. 9), and total REE contents of the rocks vary between 21 and 32 ppm (Table 5). In contrast, the centimeter-size alteration patches have significantly lower REE contents, 13 to 18 ppm, and show strong positive Eu-anomalies (Fig. 10). Total REE contents show strong positive correlations with some indices of differentiation (Zr, Y, TiO_2, and P_2O_5), but exhibit no correlation with other differentiation indicators (e.g., Mg number, SiO_2, Sr, and $CaO/CaO + Na_2O$). The patches generally contain 2–20 volume percent (vol%) amygdules filled with secondary minerals, but dilution of igneous REE contents by REE-poor secondary minerals filling primary pore space cannot account for the 50% depletions of REE (and other trace elements) observed in many of the patches.

One possibility for these trace and minor element variations is that they represent the effects of hydrothermal alteration, with leaching of REE, Zr, Y, Ti, and P by hydrothermal fluids. The patches in Leg 140 rocks generally contain 2–20 vol% amygdules surrounded by a halo of intensively altered host rock. The high degree of alteration of the host

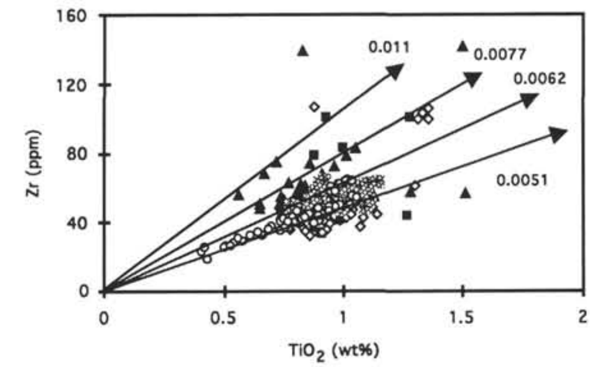

Figure 8. Zr vs. TiO_2 of Leg 69, 70, 83, 111, and 140 samples. Solid square = Leg 69, (Hubberten et al., 1983); open diamond = Leg 70, (Hubberten et al., 1983); solid triangle = Leg 83, (Emmermann, 1985); cross = Leg 111, (Naujoks, 1990); open circle = Leg 140, this study.

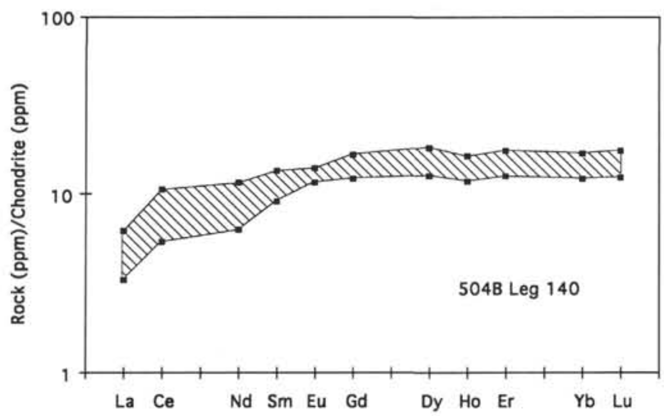

Figure 9. Chondrite-normalized rare earth element distribution (REE) of Leg 140 whole-rock samples with different amounts of alteration (Chondrite values: Evensen et al., 1978).

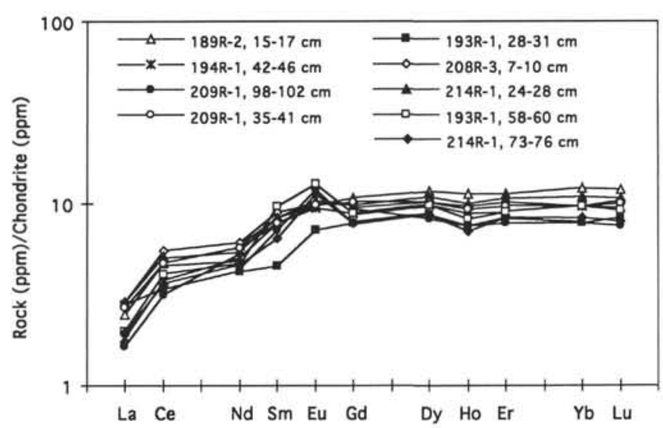

Figure 10. Chondrite-normalized rare earth element distribution (REE) of patch-rich samples of Leg 140 (Chondrite values: Evensen et al., 1978).

rock is attributed to greater primary pore space, which, when filled with hydrothermal fluids, facilitated recrystallization of the rock. Ti, Y, and total REE contents exhibit increased scatter to low values at high degrees of alteration (Fig. 11), consistent with the hypothesis of leaching of these elements during hydrothermal alteration. Zr and P contents exhibit scatter to both low and high values at increasing

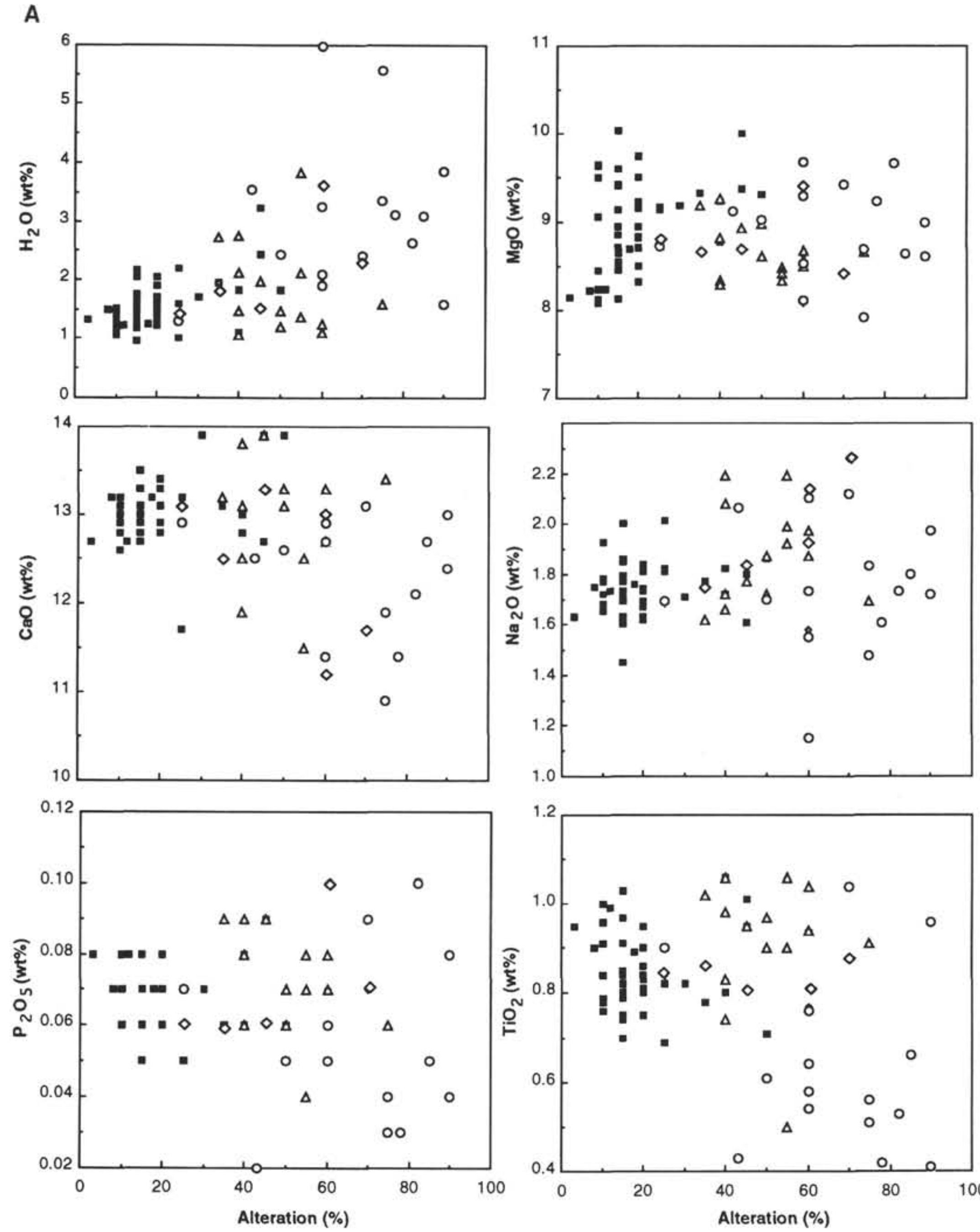

Figure 11. Major element oxides (wt%) (**A**) and trace elements (ppm) (**B**) vs. percentage of alteration for Leg 140 rocks. Symbols as in Figure 5. Arrows indicate samples that plot off scale.

intensity of alteration (Fig. 11); however, both losses and gains of these elements suggest that hydrothermal alteration processes must be more complicated. At similar degrees of alteration, the alteration halos do not exhibit the losses of REE, Y, Zr, Ti, and P that are seen in the alteration patches (Fig. 11), suggesting either that different alteration processes occurred in patches and halos, or that hydrothermal alteration may not be responsible for the trace element depletions in the patches. The secondary mineralogy of patches and halos is generally similar (Shipboard Scientific Party, 1992; Alt et al., this volume; Laverne et al., this volume), indicating that alteration processes did not differ significantly between these two portions of the rocks. Moreover, alteration halos bordering veins would seem to be sites of more efficient leaching of elements, which could be removed by solutions circulating in the vein. In contrast, leaching of elements from the alteration patches appears more difficult, because they are isolated from circulating solutions and the only means of removal of elements would be by diffusion through intergranular porosity and permeability. Although some of the chemical changes occurring in the alteration patches are probably due to hydrothermal alteration, it appears unlikely that all of the trace and minor element depletions exhibited by many of the alteration patches are the results of hydrothermal alteration (particularly Ti, Zr, Y, and REE, which are generally considered to be immobile; Pearce and Norry, 1979; Gillis et al., 1992).

Another possible explanation for this feature is that the patches originally had a smaller proportion of highly differentiated, late-stage

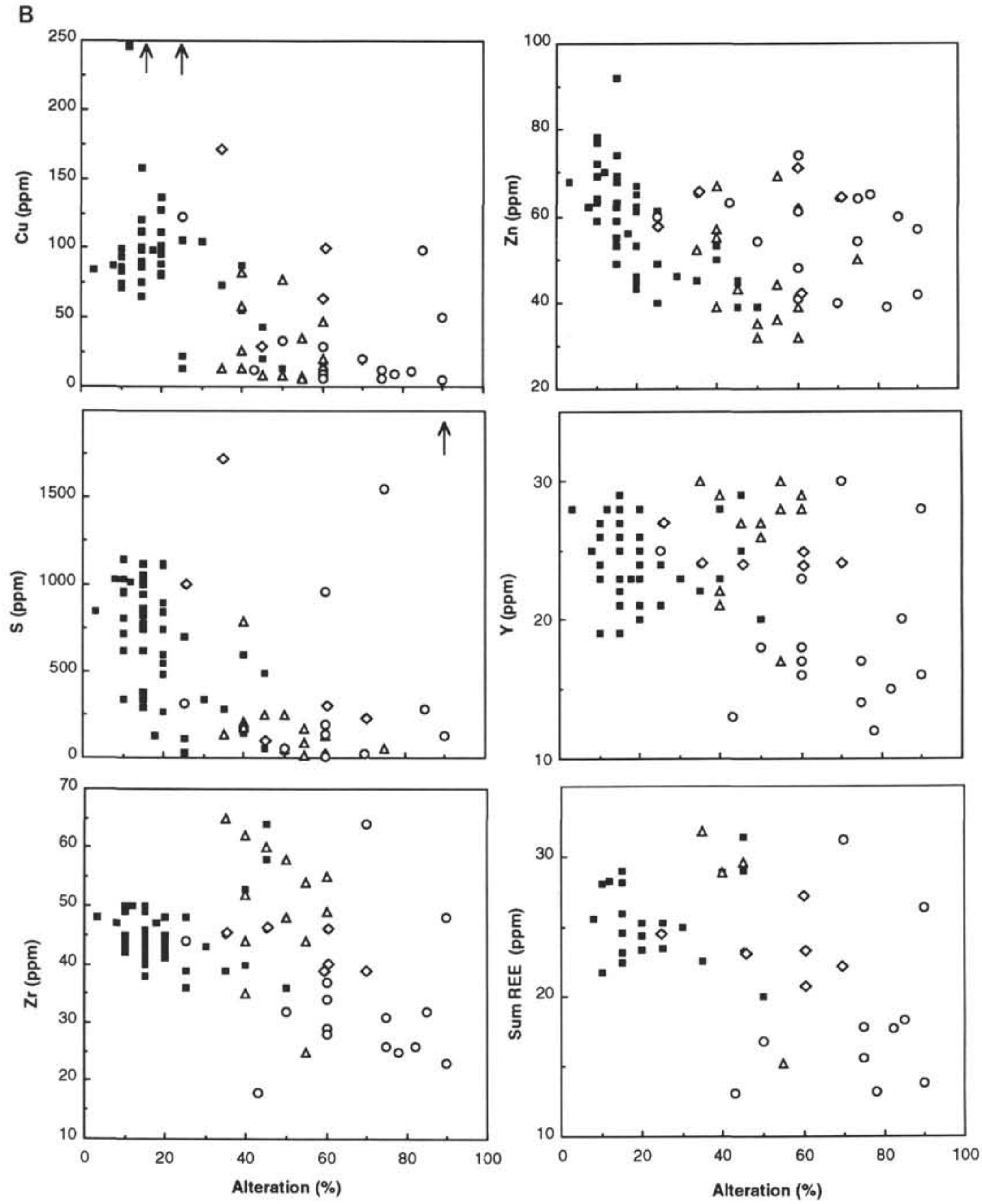

Figure 11 (continued).

magmatic liquids trapped than the surrounding rock had. Such late-stage magmatic liquids are described by the Shipboard Scientific Party (1992) as interstitial pockets of granophyric intergrowths of quartz + albite, with minor pyroxene, apatite, and Fe-Ti oxides, and sulfide mineral inclusions. These are known to be strongly enriched in incompatible elements, showing a negative Eu-anomaly. The quantitative XRD phase analysis indicates that quartz occurs in fresh samples only, consistent with occurrence of these pockets only in the patch-free rocks. The round to irregularly shaped amygdules may represent gas (CO_2) exsolution in some cases, but are more likely diktytaxitic vugs, produced by shrinkage during crystallization and cooling of the melt. Exclusion of the late-stage highly differentiated interstitial melt may in some way be related to formation of these vugs, perhaps as the result of exclusion by a CO_2-rich volatile phase. These portions of rocks have a higher permeability due to the high percentage of vugs, leading to more intense recrystallization during hydrothermal alteration. The observed positive Eu-anomalies in the patches are likely caused by the extensive recrystallization of plagioclase, which typically exhibits strong positive Eu-anomalies.

Similar intensively altered patches occur in the upper dike sections in Hole 504B, and the same types of chemical changes have been described in those samples (Alt and Emmermann, 1985; Alt et al., 1989). The chemical differences between the patches and the host rocks were simply attributed to hydrothermal alteration in those studies, but after further evaluation, we think that the main depletion of Ti, Zr, Y, and REE in these zones is a primary igneous effect, although certainly some chemical changes occurred during hydrothermal alteration (see below).

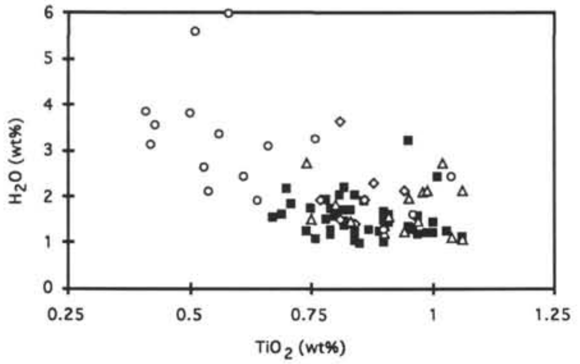

Figure 12. H_2O^+ vs. TiO_2 of Leg 140 diabases. Refer to Figure 5 for explanation of symbols.

Chemical Effects of Hydrothermal Alteration

Despite the presence of magmatic variations in composition, plots of element and oxide concentrations vs. depth and percentage of alteration reveal the effects of hydrothermal alteration in Leg 140 rocks (Figs. 5, 11, and 12). H_2O^+ contents exhibit a general trend to increasing values at greater degrees of alteration. The H_2O^+ contents of the fresh samples are between 1 and 2 wt%, whereas the more altered samples contain up to 6 wt% water. The samples with more than 2 wt% H_2O^+ are mainly alteration patches, and occur in three different zones located between 1650 and 1700, 1780 and 1830, and around 1920 mbsf (Fig. 5A). These three zones correlate with maxima in the abundance of alteration patches logged in the recovered core, and are characterized by maxima of porosity and natural remanent magnetization (NRM) inclination, and by minima of bulk density and velocity (Scientific Shipboard Party, 1992).

The rocks do not exhibit any increase in MgO with increasing alteration (Fig. 11), as is predicted from experimental seawater-basalt reactions at temperatures of 250°–350°C (e.g., Seyfried, 1987). The general lack of Mg uptake by the rocks is consistent with low seawater/rock ratios, and may be attributed at least in part to loss of Mg from circulating fluids during prior reaction with rock in the shallower portions of the hydrothermal system. Many patches, halos, and more intensively altered rocks exhibit trends toward losses of CaO and gains of Na_2O as the result of alteration of primary plagioclase to albite and oligoclase. Other patches have lost CaO with no Na_2O gain, and one sample has lost both CaO and Na_2O. The latter reflects the abundance of chlorite and extensive alteration of both pyroxene and plagioclase in the sample. Despite trends of P_2O_5 depletion that are attributed to igneous variations (see above), P_2O_5 contents exhibit increased scatter to both high and low values at high degrees of alteration (Fig. 11), consistent with mobility of P and the presence of traces of secondary apatite in the rocks (Laverne et al., this volume; J. Alt, unpubl. data). The apparent TiO_2 losses at high degrees of alteration (Fig. 11) are mainly attributed to primary igneous depletions in the patches, but some loss or local mobility of Ti is probable in the more highly altered samples, given the intensive alteration of titanomagnetite to titanite in these samples.

Zn contents decrease progressively with depth starting from 1650 mbsf (Fig. 5B). This is attributed to breakdown of clinopyroxene to amphibole and loss of Zn, which was originally contained in pyroxene, to hydrothermal fluids. This effect is also seen as a general decrease of Zn contents with increasing alteration in the "fresh" dark gray samples, with no significant further decrease in Zn contents in the more highly altered patches (Fig. 11). The most altered samples (halos and patches) generally show a strong depletion of Cu (<20 ppm), compared with the mean value of the least altered samples (including the host rocks for patches and halos), which is around 90 ppm (Figs. 5C, 11). Samples depleted in Cu contain only traces of sulfide minerals, reflecting a leaching of metals (Cu) and sulfides from the rocks by hydrothermal fluids and leading to generally low S contents (Fig. 11). Despite loss of metal sulfides from the rocks, many of the low-Cu patches have high S contents because of the later formation of secondary anhydrite in small veinlets and replacement by plagioclase in the rocks during seawater recharge.

The rocks recovered from the lower sheeted dike complex of Hole 504B on Leg 140 are distinguished from the overlying dikes by losses of metals and sulfur from the rocks, by greater proportions of amphibole, and the presence of hornblende and secondary anorthite in addition to actinolite and albite, vs. mainly actinolite and albite in the upper dikes. The secondary mineralogy, as well as oxygen isotope ratios, indicates higher temperatures of hydrothermal alteration in the lower dikes (Laverne et al., this volume; Alt et al., this volume). This led to a more intensive recrystallization of the rocks and losses of metals and sulfur, which are more soluble in hydrothermal fluids at temperatures above 350°C (Seyfried, 1987; Seewald and Seyfried, 1990). These effects are similar to those observed in the lower sheeted dikes in ophiolites (Baragar et al., 1990; Alt, unpubl. data). If 40 ppm Zn and 50 ppm Cu are lost from 500 m of lower dikes, these losses can account for the Zn and Cu enrichments observed in the sulfide mineralization in the transition zone in Hole 504B (mean values of 165 and 150 ppm, respectively; Alt et al., 1986). The lower sheeted dikes in the ocean crust are thus likely a major source for metals and sulfur, which are transported by hydrothermal fluids to vents at the seafloor and form sulfide deposits on and within the seafloor.

SUMMARY AND CONCLUSIONS

Rocks from the lower sheeted dike complex in Hole 504B sampled during Leg 140 are relatively uniform in composition and similar to rocks from the shallower portions of the sheeted dike section of the hole. They are moderately evolved MORB with relatively high MgO contents (7.9–10 wt%) and Mg numbers (0.60–0.70), and have unusually low incompatible element contents (TiO_2 = 0.42–1.1 wt%, Zr = 23–62 ppm). The rocks exhibit some compositional variations, however, reflecting varying degrees of differentiation, and olivine and plagioclase accumulation in the rocks. Discrete compositional intervals in the hole may be related to injection of packets of dikes with similar compositions. Systematic depletions of total REE, Zr, Y, TiO_2, and P_2O_5 in centimeter-size alteration patches are most likely attributed to a lack of highly differentiated late-stage interstitial liquids, rich in incompatible elements, from small portions of the rocks, and are probably related to the formation of diktytaxitic vugs during cooling and crystallization. These vugs enhanced the porosity of the rocks, leading to the extensively altered patches surrounding the vugs and further chemical differences from the host rocks.

All of the Leg 140 rocks are affected by a pervasive background alteration, and are 2%–20% recrystallized. More intensive alteration (up to 80%–100%) occurred where fluids had greater access to the rocks (i.e., in alteration halos around veins and in isolated alteration patches). As a result of hydrothermal alteration and formation of secondary hydrous phases, the rocks exhibit increased H_2O^+. Local gains of Na_2O and losses of CaO are related to replacement of primary plagioclase by albite and oligoclase, although secondary anorthite is also present. Slight positive Eu anomalies in more altered samples are attributed to the formation of secondary plagioclase. Some mobility of P_2O_5 led to minor increases and decreases in P_2O_5 contents. Although most variations in TiO_2 are probably related to igneous processes, some mobility of Ti may have occurred locally as the result of intensive alteration of titanomagnetite to titanite. Higher temperatures of alteration in the lower sheeted dikes led to the breakdown of pyroxene and sulfide minerals and losses of Zn, Cu, and S to hydrothermal fluids. Later addition of anhydrite to the rocks in microfractures and replacing plagioclase caused local increases in sulfur. The lower sheeted dikes are a major source of metals to hydrothermal fluids for the formation of metal sulfide deposits on and within the seafloor.

ACKNOWLEDGMENTS

The authors wish to thank W. Bach for his numerous helpful discussion and his critical review. We also wish to thank the reviewers J.E. Dixon and P.T. Robinson for their critical and helpful contributions. We also are very grateful to M. Keβler and R. Zier for their assistance in performing the chemical analysis. M. Grünhäuser did the XRF measurements, T. Umsonst the XRD measurements, and S. Schmidt helped perform the S, H_2O, and REE analysis. The research was supported by the Deutsche Forschungsgemeinschaft, Bonn-Bad Godesberg, Federal Republic of Germany (Er 123/6-1+2), and by a grant from JOI-USSAC.

REFERENCES*

Alt, J.C., Anderson, T.F., Bonnell, L., and Muehlenbachs, K., 1989. Mineralogy, chemistry, and stable isotopic compositions of hydrothermally altered sheeted dikes: ODP Hole 504B, Leg 111. *In* Becker, K., Sakai, H., et al., *Proc. ODP, Sci. Results,* 111: College Station, TX (Ocean Drilling Program), 27–40.

Alt, J.C., and Emmermann, R., 1985. Geochemistry of hydrothermally altered basalts: Deep Sea Drilling Project Hole 504B. *In* Anderson, R.N., Honnorez, J., Becker, K., et al., *Init. Repts. DSDP,* 83: Washington (U.S. Govt. Printing Office), 249–262.

Alt, J.C., Honnorez, J., Laverne, C., and Emmermann, R., 1986. Hydrothermal alteration of a 1 km section through the upper oceanic crust, Deep Sea Drilling Project Hole 504B: mineralogy, chemistry, and evolution of seawater-basalt interactions. *J. Geophys. Res.,* 91:10309–10335.

Autio, L.K., and Rhodes, J.M., 1983. Costa Rica Rift Zone basalts: geochemical and experimental data from a possible example of multistage melting. *In* Cann, J.R., Langseth, M.G., Honnorez, J., Von Herzen, R.P., White, S.M., et al., *Init. Repts. DSDP,* 69: Washington (U.S. Govt. Printing Office), 729–745.

Autio, L.K., Sparks, J.W., and Rhodes, J.M., 1989. Geochemistry of Leg 111 basalts: intrusive feeders for highly depleted pillows and flows. *In* Becker, K., Sakai, H., et al., *Proc. ODP, Sci. Results,* 111: College Station, TX (Ocean Drilling Program), 3–16.

Baragar, W.R.A., Lambert, M.B., Baglow, N., and Gibson, I.L, 1990. The sheeted dyke zone in the Troodos Ophiolite. *In* Malpas, J., Moores, E.M., Panayiotou, A., Xenophontos, C. (Eds.), *Ophiolites: Oceanic Crustal Analogues,* 37–51.

Emmermann, R., 1985. Basement geochemistry, Hole 504B. *In* Anderson, R.N., Honnorez, J., Becker, K., et al., *Init. Repts. DSDP,* 83: Washington (U.S. Govt. Printing Office), 183–199.

Emmermann, R., and Lauterjung, J., 1990. Double X-ray analysis of cuttings and rock flour: a powerful tool for rapid and reliable determination of borehole lithostratigraphy. *Sci. Drill.,* 1:269–282.

Evensen, N.M., Hamilton, P.J., and O'Nions, R.K., 1978. Rare-earth abundances on chondritic meteorites. *Geochim. Cosmochim. Acta.,* 42:1199–1212.

Fox, P.J., and Stroup, J., 1981. The plutonic foundation of the oceanic crust. *In* Emiliani, C. (Ed.), *The Sea* (The Oceanic Lithosphere): New York (Wiley), 119–218.

Gillis, K.M., Ludden, J.N., and Smith, A.D., 1992. Mobilization of REE during crustal aging in the Troodos Ophiolite, Cyprus. *Chem. Geol.,* 98:71–86.

Govindaraju, K., 1989. 1989 compilation of working values and sample description for 272 geostandards. *Geostand. Newsl.,* 13:1–113.

Hubberten, H.-W., Emmermann, R., and Puchelt, H., 1983. Geochemistry of basalts from Costa Rica Rift Sites 504 and 505 (Deep Sea Drilling Project Legs 69 and 70). *In* Cann, J.R., Langseth, M.G., Honnorez, J., Von Herzen, R.P., White, S.M., et al., *Init. Repts. DSDP,* 69: Washington (U.S. Govt. Printing Office), 791–803.

Natland, J.H., Adamson, A.C., Laverne, C., Melson, W.G., and O'Hearn, T.O., 1983. A compositionally nearly steady-state magma chamber at the Costa Rica Rift: evidence from basalt glass and mineral data, Deep Sea Drilling Project Sites 501, 504, and 505. *In* Cann, J.R., Langseth, M.G., Honnorez, J., Von Herzen, R.P., White, S.M., et al., *Init. Repts. DSDP,* 69: Washington (U.S. Govt. Printing Office), 811–858.

Naujoks, F., 1990. Geochemie und hydrothermale Alteration des Sheeted-Dike-Komplexes in DSDP Bohrung 504B am Costa Rica Rift [Dipl. arbeit]. Univ. Giessen.

Pearce, J.A., and Norry, M.J., 1979. Petrogenetic implications of Ti, Zr, Y and Nb variations in volcanic rocks. *Contrib. Mineral. Petrol.,* 69:33–47.

Raitt, R.W., 1963. The crustal rocks. *In* Hill, M. (Ed.), *The Sea: Ideas and Observations on Progress in the Study of the Seas:* New York (Wiley-Interscience), 3:85–102.

Seewald, J.S., and Seyfried, W.E., Jr., 1990. The effect of temperature on metal mobility in subseafloor hydrothermal systems: constraints from basalt alteration experiments. *Earth Planet. Sci. Lett.,* 101:388–403.

Seyfried, W.E., Jr., 1987. Experimental and theoretical constraints on hydrothermal alteration processes at mid-ocean ridges. *Annu. Rev. Earth Planet. Sci.,* 15:317–335.

Shipboard Scientific Party, 1988. Site 504: Costa Rica Rift. *In* Becker, K., Sakai, H., et al., *Proc. ODP, Init. Repts.,* 111: College Station, TX (Ocean Drilling Program), 35–251.

————, 1992. Site 504. *In* Dick, H.J.B., Erzinger, J., Stokking, L.B., et al., *Proc. ODP, Init. Repts.,* 140: College Station, TX (Ocean Drilling Program), 37–200.

Zuleger, E., and Erzinger, J., 1988. Determination of the REE and Y in silicate materials with ICP-AES. *Fresenius' Z. Anal. Chem.,* 332:140–143.

* Abbreviations for names of organizations and publications in ODP reference lists follow the style given in *Chemical Abstracts Service Source Index* (published by American Chemical Society).

Date of initial receipt: 26 April 1993
Date of acceptance: 11 January 1994
Ms 137/140SR-022

Table 1. Major and trace element composition of Hole 504B diabases, recovered during Legs 137/140.

Leg:	137	137	137	137	137	137	137	140	140	140	140	140
Core-section:	173 R01	173 R01	174 R02	177 R01	181 M1	181 M2	186 R02	187 R01	187 R01	189 R01	189 R01	189 R01
Interval (cm):	54–57	73–76	23–26	48–51	6–10	95–97	30–32	59–63A	59–63B	85–88	90–94A	90–94B
Piece no.:	6	9	5	13	1	7B	8	14	14	19	20	20
Depth (mbsf):	1570.5	1570.7	1578.0	1605.0	1620.5	1622.8	1628.1	1632.6	1632.6	1651.9	1651.9	1651.9
Lithologic unit*:	193	193	195	202	204	208	213	216	216	218	218	218
Unit rock name:	OPC	OPC	OPC	OPC	OPC	OPC	AD	sPCD	sPCD	mPOCD	mPOCD	mPOCD
Alteration (%):	3	40	10	15	10	25	35	25	90	12	15	60
Alteration type:	D	L	D	D	D	P	L	D	P	D	D	H
SiO_2 (wt%)	50.1	50.7	50.6	51.0	49.6	50.7	47.1	50.4	50.6	50.5	50.5	49.9
TiO_2	0.95	0.74	1.00	1.03	1.00	0.90	1.02	0.96	0.82	0.99	0.97	0.81
Al_2O_3	14.9	15.5	14.8	14.8	14.6	14.9	16.2	15.3	14.8	15.1	15.1	15.2
Fe_2O_3	2.79	2.36	2.98	2.81	2.72	2.27	2.14	2.41	2.21	2.68	2.54	2.00
FeO	7.30	7.08	7.40	7.64	7.54	7.32	7.16	7.10	8.18	7.31	7.34	7.83
MnO	0.17	0.16	0.18	0.18	0.18	0.18	0.17	0.18	0.17	0.18	0.18	0.17
MgO	8.14	8.33	8.13	8.71	8.23	8.72	9.18	8.61	8.75	8.24	8.44	8.63
CaO	12.7	11.9	12.6	12.7	13.0	12.9	13.2	13.0	11.7	12.7	12.8	11.2
Na_2O	1.63	2.19	1.66	1.73	1.68	1.69	1.62	1.97	2.01	1.73	1.77	2.13
P_2O_5	0.08	0.06	0.08	0.08	0.07	0.07	0.09	0.08	0.07	0.08	0.08	0.07
H_2O^+	1.33	2.74	1.21	1.24	1.43	1.29	2.73	1.60	2.19	1.22	1.56	3.65
Sum	100.1	101.8	100.6	101.9	100.1	100.9	100.6	101.6	101.5	100.7	101.3	101.6
Fe_2O_{3T}	10.9	10.2	11.2	11.3	11.1	10.4	10.1	10.3	11.3	10.8	10.7	10.7
S (ppm)	842	191	718	379	334	316	139	131	30	1015	740	308
Cr	243	247	221	178	226	302	348	284	257	255	278	320
Ni	87	89	85	80	84	92	134	90	94	88	92	93
Cu	84	26	83	65	74	122	13	50	13	246	98	63
Zn	68	67	72	69	69	60	52	57	61	70	69	71
Ga	15	14	14	16	14	15	15	16	15	14	17	15
Sr	46	54	47	47	45	45	66	51	54	48	48	54
Y	28	21	27	28	27	25	30	28	24	28	29	23
Zr	48	35	50	50	49	44	65	48	39	50	49	39
FM	54.6	52.5	55.3	53.9	54.8	51.8	49.7	51.8	53.7	54.1	53.3	52.7
Mg#	0.60	0.62	0.59	0.60	0.59	0.62	0.64	0.62	0.61	0.60	0.61	0.62
Ox	25.6	23.1	26.6	24.9	24.5	21.8	21.2	23.4	19.6	24.8	23.8	18.7
Y/Zr	0.58	0.60	0.54	0.56	0.55	0.57	0.46	0.58	0.62	0.56	0.59	0.59
Zr/TiO_2	0.0051	0.0047	0.0050	0.0049	0.0049	0.0049	0.0064	0.0050	0.0048	0.0051	0.0051	0.0048

Notes: * = Shipboard Scientific Party (1992). $K_2O < 0.05\%$; $CO_2 < 0.1\%$; Rb, Pb, Th < 5 ppm; Ba < 20 ppm. Unit rock name: m = moderately; s = sparsely; O = Olivine; P = plagioclase; C = clinopyroxene; D = diabase; A = aphyric. Alteration type: D = macroscopically dark, less altered diabase; L = macroscopically light, high background alteration; H = diabase containing high percentage of halos around veins; P = samples with green patches or vugs and a high background alteration. n.d. = not determined. $FM = FeO_{total}/(FeO_{total} + MgO) \cdot 100$; Mg# = MgO/MgO + FeO (molar); $Ox = Fe_2O_3 \cdot 100/Fe_2O_{3T}$.

Table 1 (continued).

Leg:	140	140	140	140	140	140	140	140	140	140	140	140
Core-section:	189 R02	190 R01	193 R01	193 R01	193 R01	193 R01	194 R01	194 R01	195 R01	196 R01	197 R01	197 R01
Interval (cm):	15–17	10–14	22–24	28–31	44–46	58–60 B	36–40	42–46	1–3	21–26	29–31	116–120
Piece no.:	3	2	7	9	13A	14	7	8	1	4	7	26
Depth (mbsf):	1653.5	1655.2	1674.7	1674.8	1675.0	1675.1	1680.8	1680.8	1690.3	1696.7	1703.1	1704.0
Lithologic unit*:	218	218	220	220	220	220	220	220	221	222	222	223
Unit rock name:	mPOCD	mPOCD	mPOCD	mPOCD	mPOCD	mPOCD	mPOCD	mPOCD	mPOCD	mPOCD	mPOCD	sPOCD
Alteration (%):	85	60	60	43	60	75	20	55	10	15	70	20
Alteration type:	P	P	P	P	H	P	D	P	D	D	H	D
SiO_2 (wt%)	50.5	50.8	50.3	50.5	50.2	50.2	50.0	50.5	50.0	50.5	50.1	48.6
TiO_2	0.66	0.58	0.76	0.43	0.94	0.51	0.95	0.50	0.91	0.97	0.88	0.81
Al_2O_3	15.7	14.4	14.9	15.6	15.4	14.5	15.5	14.8	15.6	15.4	15.2	16.2
Fe_2O_3	1.67	1.38	2.05	1.80	2.43	1.38	2.80	1.34	2.49	2.88	2.34	2.85
FeO	6.69	7.49	7.87	6.48	6.72	7.04	6.84	7.61	7.03	6.95	7.88	6.25
MnO	0.16	0.16	0.17	0.15	0.19	0.13	0.18	0.16	0.17	0.18	0.17	0.16
MgO	8.64	8.11	8.52	9.12	8.08	7.92	8.32	8.42	8.07	8.12	8.39	9.23
CaO	12.7	11.4	11.4	12.5	13.0	10.9	12.9	11.5	12.8	12.9	11.7	13.1
Na_2O	1.80	1.15	2.10	2.06	1.93	1.48	1.74	1.99	1.93	1.86	2.26	1.62
P_2O_5	0.05	0.05	0.06	0.02	0.10	0.04	0.08	0.04	0.07	0.08	0.07	0.06
H_2O^+	3.09	5.98	3.25	3.55	2.12	5.57	1.29	3.82	1.45	1.18	2.31	2.04
Sum	101.7	101.5	101.4	102.2	101.1	99.7	100.6	100.7	100.5	101.0	101.3	100.9
Fe_2O_{3T}	9.1	9.7	10.8	9.0	9.9	9.2	10.4	9.8	10.3	10.6	11.1	9.8
S (ppm)	282	135	192	n.d.	n.d.	1550	1120	170	800	293	231	544
Cr	327	299	252	402	278	393	313	334	259	249	292	346
Ni	100	92	88	113	97	100	100	105	87	86	92	138
Cu	98	12	29	12	101	6	80	7	71	111	18	95
Zn	60	61	74	63	62	64	67	69	78	55	64	61
Ga	15	13	15	n.d.	n.d	13	15	13	16	15	15	13
Sr	55	33	57	51	49	39	49	49	50	50	57	51
Y	20	16	23	13	25	17	26	17	27	27	24	23
Zr	32	29	37	18	46	26	48	25	45	49	39	41
FM	48.7	51.8	53.3	47.0	52.4	51.1	52.9	51.2	53.5	54.0	54.3	48.9
Mg#	0.65	0.62	0.61	0.67	0.62	0.63	0.61	0.63	0.61	0.60	0.60	0.65
Ox	18.3	14.2	19.0	20.0	24.6	15.0	26.9	13.7	24.2	27.1	21.1	29.1
Y/Zr	0.63	0.55	0.62	0.72	0.54	0.65	0.54	0.68	0.60	0.55	0.62	0.56
Zr/TiO_2	0.0048	0.0050	0.0049	0.0042	0.0049	0.0051	0.0051	0.0050	0.0049	0.0051	0.0044	0.0051

Table 1 (continued).

Leg:	140	140	140	140	140	140	140	140	140	140	140	140
Core-section:	197 R01	198 R01	198 R01	199 R01	199 R01	200 R01	200 R02	200 R02	200 R03	200 R04	202 R01	202 R01
Interval (cm):	123–126	50–54	79–82	54–57	89–92	35–39	53–57	116–119	115–117	16–19	9–12	23–25
Piece no.:	27	14	20	13	21	8	7B	18	18	4	3	7
Depth (mbsf):	1704.0	1712.7	1713.0	1719.9	1720.3	1729.0	1730.6	1731.3	1732.8	1733.3	1747.3	1747.4
Lithologic unit*:	223	223	224	226	226	227	227	227	227	227	229	229
Unit rock name:	sPOCD	sPOCD	AD	mPOCD	mPOCD	mPOCD	mPOCD	mPOCD	mPOCD	mPOCD	sPOCD	sPOCD
Alteration (%):	15	20	75	15	15	10	10	10	15	20	10	25
Alteration type:	D	D	L	D	D	D	D	D	D	L	D	H
SiO_2 (wt%)	49.1	49.3	49.4	49.4	48.3	50.0	49.4	49.2	48.2	49.1	49.4	49.7
TiO_2	0.80	0.83	0.91	0.79	0.75	0.79	0.76	0.78	0.70	0.75	0.84	0.84
Al_2O_3	16.0	15.8	15.6	16.4	15.8	16.6	16.5	16.2	16.4	16.2	15.7	15.7
Fe_2O_3	2.69	2.61	2.27	2.20	1.67	1.92	2.37	2.10	1.72	1.97	2.13	1.67
FeO	6.49	6.74	6.87	6.30	7.23	6.46	5.97	6.57	6.55	6.33	7.17	7.50
MnO	0.16	0.17	0.17	0.16	0.17	0.15	0.15	0.17	0.16	0.15	0.18	0.20
MgO	9.41	9.51	8.66	9.60	9.43	9.63	9.65	9.50	10.04	9.75	9.05	8.77
CaO	13.0	12.8	13.4	13.0	12.7	13.2	13.1	13.2	12.8	13.1	12.9	13.1
Na_2O	1.63	1.67	1.69	1.71	1.60	1.72	1.68	1.65	1.45	1.63	1.77	1.68
P_2O_5	0.06	0.06	0.06	0.06	0.05	0.06	0.06	0.06	0.05	0.06	0.07	0.06
H_2O^+	1.71	1.41	1.59	1.27	1.75	1.18	1.09	1.51	2.16	1.51	1.06	1.40
Sum	101.1	100.9	100.6	100.9	99.5	101.7	100.7	100.9	100.2	100.6	100.3	100.6
Fe_2O_{3T}	9.9	10.1	9.9	9.2	9.7	9.1	9.0	9.4	9.0	9.0	10.1	10.0
S (ppm)	338	596	58	1005	860	1030	956	621	770	839	1140	1000
Cr	355	336	443	367	382	374	388	377	378	381	339	339
Ni	150	146	105	158	160	157	158	154	191	161	123	117
Cu	112	101	9	88	386	86	86	99	75	88	93	503
Zn	68	62	50	63	74	59	63	77	92	65	64	58
Ga	15	14	16	14	13	14	13	14	13	13	14	14
Sr	50	53	62	65	62	67	67	66	61	65	55	52
Y	25	23	26	19	22	19	19	23	21	20	24	27
Zr	41	43	44	43	42	42	42	43	38	41	44	44
FM	48.6	48.9	50.7	46.3	48.1	46.0	45.6	47.1	44.6	45.4	50.1	50.6
Mg#	0.65	0.65	0.63	0.67	0.66	0.68	0.68	0.67	0.69	0.68	0.64	0.63
Ox	27.1	25.8	22.9	23.9	17.2	21.1	26.3	22.3	19.1	21.8	21.1	16.7
Y/Zr	0.61	0.53	0.59	0.44	0.52	0.45	0.45	0.53	0.55	0.49	0.55	0.61
Zr/TiO_2	0.0051	0.0052	0.0048	0.0054	0.0056	0.0053	0.0055	0.0055	0.0054	0.0055	0.0052	0.0052

Table 1 (continued).

Leg:	140	140	140	140	140	140	140	140	140	140	140	140
Core-section:	203 R01	204 R01	204 R01	205 R01	207 R01	208 R01	208 R01	208 R02	208 R03	209 R01	209 R01	209 R01
Interval (cm):	12–14	0–4	15–19	21–23	22–26	88–91	110–114	0–6	7–10	35–41 A	35–41B	98–102
Piece no.:	4	1	4	3	6	19	23	1	1	6A	6A	14
Depth (mbsf):	1749.1	1756.5	1756.7	1757.2	1768.6	1778.9	1779.1	1779.5	1781.1	1787.9	1787.9	1788.5
Lithologic unit*:	231	232	232	232	236	239	239	239	239	240	240	240
Unit rock name:	AD	sPCOD	sPCOD	sPCOD	AD	mOPCD	mOPCD	mOPCD	mOPCD	mOPCD	mOPCD	mOPCD
Alteration (%):	15		45	40	40	35	18	40	75	15	50	78
Alteration type:	D	L	L	L	D	H	D	L	P	D	P	P
SiO_2 (wt%)	49.5	48.0	48.7	48.1	50.5	49.4	50.2	50.0	50.0	49.1	49.0	49.3
TiO_2	0.91	0.99	0.95	0.98	1.06	0.86	0.89	0.83	0.56	0.79	0.61	0.42
Al_2O_3	15.2	15.8	15.3	15.9	14.1	16.0	15.9	16.0	16.4	17.9	17.2	15.9
Fe_2O_3	2.35	2.48	2.43	2.18	2.28	2.51	2.44	2.29	2.09	1.75	1.70	2.07
FeO	7.33	6.95	6.36	6.14	7.85	7.19	6.62	6.76	7.12	6.16	6.93	8.22
MnO	0.19	0.16	0.15	0.15	0.19	0.17	0.17	0.17	0.16	0.14	0.15	0.16
MgO	8.94	9.23	8.92	9.26	8.76	8.66	8.69	8.82	8.69	8.54	9.03	9.23
CaO	13.1	13.8	13.9	13.8	12.8	12.5	13.2	13.1	11.9	13.3	12.6	11.4
Na_2O	1.85	1.58	1.77	1.66	1.82	1.74	1.76	1.72	1.83	1.73	1.70	1.61
P_2O_5	0.07	0.09	0.09	0.09	0.08	0.06	0.07	0.06	0.03	0.07	0.05	0.03
H_2O^+	1.62	2.12	1.98	2.11	1.10	1.95	1.25	1.48	3.36	1.74	2.44	3.12
Sum	101.1	101.2	100.6	100.4	100.5	101.0	101.2	101.2	102.1	101.2	101.4	101.5
Fe_2O_{3T}	10.5	10.2	9.5	9.0	11.0	10.5	9.8	9.8	10.0	8.6	9.4	11.2
S (ppm)	619	60	245	212	142	1730	128	784	n.d.	1010	56	n.d.
Cr	364	362	357	346	273	369	337	341	396	312	365	413
Ni	105	135	120	137	90	109	102	108	125	128	126	128
Cu	158	8	8	13	55	171	98	82	12	120	33	9
Zn	62	46	43	57	50	65	56	55	54	49	54	65
Ga	16	16	15	15	14	15	14	15	n.d.	14	14	13
Sr	53	67	70	68	55	55	59	57	57	60	55	50
Y	27	29	27	29	28	24	23	22	14	23	18	12
Zr	46	62	60	62	53	45	47	44	31	43	32	25
FM	51.4	49.9	48.9	46.7	53.0	52.2	50.4	50.0	50.9	47.5	48.4	52.2
Mg#	0.63	0.64	0.65	0.67	0.61	0.62	0.64	0.64	0.63	0.66	0.66	0.62
Ox	22.4	24.3	25.6	24.2	20.7	23.9	24.9	23.3	20.9	20.4	18.1	18.4
Y/Zr	0.59	0.47	0.45	0.47	0.53	0.53	0.49	0.50	0.45	0.53	0.56	0.48
Zr/TiO_2	0.0051	0.0063	0.0063	0.0063	0.0050	0.0052	0.0053	0.0053	0.0055	0.0054	0.0052	0.0060

Table 1 (continued).

Leg:	140	140	140	140	140	140	140	140	140	140	140	140
Core-section:	209 R01	209 R02	210 R01	210 R01	211 R01	213 R01	214 R01	214 R01	214 R01	215 R01	215 R01	215 R01
Interval (cm):	129–132	68–70	33–37	80–87	70–74	64–68	24–28	36–40	73–76	39–43	59–63	81–85
Piece no.:	15	10	4C	12	16	19	5A	5	8	11	12	20
Depth (mbsf):	1788.8	1789.6	1795.2	1795.7	1799.2	1813.1	1818.9	1819.0	1819.3	1823.5	1823.6	1823.8
Lithologic unit*:	240	240	241	241	241	243	244	244	244	244	244	244
Unit rock name:	mOPCD	mOPCD	sPOCD	sPOCD	sPOCD	sPOCD	mPOCD	mPOCD	mPOCD	mPOCD	mPOCD	mPOCD
Alteration (%):	20	15	15		30	35	82	50	90	40	15	20
Alteration type:	D	D	D	D	D	D	P	D	P	L	D	D
SiO_2 (wt%)	48.9	49.1	50.0	49.9	49.2	49.1	49.1	49.4	48.8	49.4	49.2	48.6
TiO_2	0.80	0.74	0.85	0.87	0.82	0.78	0.53	0.71	0.41	0.80	0.82	0.90
Al_2O_3	17.2	17.6	16.0	15.4	16.2	16.2	15.9	17.0	13.9	15.8	15.9	15.6
Fe_2O_3	2.13	2.45	2.40	n.d.	2.40	2.21	2.20	1.38	2.07	2.05	2.38	3.17
FeO	6.09	5.53	6.57	n.d.	6.48	6.56	6.93	5.69	6.78	7.06	6.68	6.60
MnO	0.16	0.15	0.16	0.16	0.15	0.15	0.13	0.12	0.12	0.16	0.16	0.19
MgO	8.49	8.51	8.85	8.82	9.19	9.33	9.67	9.31	8.99	9.23	9.13	8.81
CaO	13.4	13.5	13.1	13.6	13.9	13.1	12.1	13.9	12.4	13.0	13.1	13.4
Na_2O	1.69	1.69	1.79	1.90	1.71	1.77	1.73	1.86	1.72	1.72	1.77	1.81
P_2O_5	0.07	0.06	0.07	0.06	0.07	0.06	0.10	0.06	0.04	0.06	0.06	0.07
H_2O^+	1.56	1.26	0.97	1.29	1.72	1.94	2.62	1.84	3.85	1.84	1.49	1.67
Sum	100.5	100.6	100.8	101.5	101.8	101.2	101.0	101.3	99.1	101.1	100.7	100.8
Fe_2O_{3T}	8.9	8.6	9.7	9.5	9.6	9.5	9.9	7.7	9.6	9.9	9.8	10.5
S (ppm)	1110	943	1050	n.d.	338	282	n.d.	37	6370	595	823	889
Cr	329	343	348	372	337	326	473	299	376	370	348	362
Ni	121	126	109	105	129	129	166	132	143	125	130	112
Cu	100	88	86	73	104	73	11	13	5	87	100	96
Zn	53	49	59	49	46	45	39	39	42	53	53	65
Ga	16	15	14	15	13	13	n.d.	13	12	14	14	14
Sr	60	61	59	56	53	53	49	56	50	51	54	56
Y	21	19	23	27	23	22	15	20	16	23	25	28
Zr	43	40	45	45	43	39	26	36	23	40	42	48
FM	48.5	47.6	49.7	49.2	48.5	47.8	47.9	42.7	49.0	49.1	49.1	51.7
Mg#	0.65	0.66	0.64	0.67	0.65	0.66	0.66	0.71	0.65	0.65	0.65	0.62
Ox	24.0	28.5	24.7		25.0	23.3	22.2	17.9	21.5	20.7	24.3	30.1
Y/Zr	0.49	0.48	0.51	0.60	0.53	0.56	0.58	0.56	0.70	0.58	0.60	0.58
Zr/TiO_2	0.0054	0.0054	0.0053	0.0052	0.0052	0.0050	0.0049	0.0051	0.0056	0.0050	0.0051	0.0053

Table 1 (continued).

Leg:	140	140	140	140	140	140	140	140	140	140	140	140
Core-section:	216 R01	218 R01	220 R01	222 R01	222 R01	222 R01	224 R01	224 R01	225 R01	225 R02	225 R02	225 R02
Interval (cm):	54–56	7–9	23–26	69–73	115–120A	115–120B	38–42	71–74	107–109	29–32	68–72A	68–72B
Piece no.:	12	2	6	12A	12	22	8	13	27	5	13	13
Depth (mbsf):	1828.4	1847.0	1865.7	1885.3	1885.8	1885.8	1904.1	1904.4	1913.3	1914.0	1914.4	1914.4
Lithologic unit*:	245	247	252	254	256	256	258	258	259	260	260	260
Unit rock name:	mCOPD	AD	mCOPD	mCOPD	AD	AD	mCPOD	mCPOD	AD	mCOPD	mCOPD	mCOPD
Alteration (%):	15	55	10	45	45	70	8	60	50	15	20	70
Alteration type:	D	L	D	D	D	P	D	L	L	D	D	H
SiO_2 (wt%)	49.2	49.7	50.4	46.8	48.0	48.4	50.0	50.9	49.5	49.6	48.9	49.5
TiO_2	0.84	1.06	0.96	0.95	1.01	1.04	0.90	1.04	0.97	0.82	0.83	0.77
Al_2O_3	16.1	14.7	15.0	16.6	16.1	15.8	15.9	14.8	15.5	16.0	16.2	15.3
Fe_2O_3	2.03	2.37	2.74	2.01	2.00	2.29	2.90	2.20	2.44	2.22	1.75	1.95
FeO	6.72	7.95	7.16	6.92	6.21	6.31	6.39	7.02	6.89	6.91	6.88	7.87
MnO	0.17	0.19	0.18	0.16	0.14	0.14	0.16	0.16	0.17	0.17	0.15	0.16
MgO	8.64	8.47	8.44	10.01	9.37	9.43	8.22	8.67	8.97	9.14	9.15	9.39
CaO	13.3	12.5	12.9	12.7	13.9	13.1	13.2	13.3	13.1	13.0	13.3	12.7
Na_2O	2.00	2.19	1.78	1.61	1.80	2.12	1.75	1.87	1.87	1.78	1.74	1.58
P_2O_5	0.07	0.08	0.07	0.09	0.09	0.09	0.07	0.08	0.07	0.07	0.07	0.06
H_2O^+	2.05	2.13	1.32	3.22	2.43	2.42	1.49	1.11	1.47	1.38	1.71	1.94
Sum	101.1	101.3	101.0	101.1	101.1	101.1	101.0	101.2	101.0	101.1	100.7	101.2
Fe_2O_{3T}	9.5	11.2	10.7	9.7	8.9	9.3	10.0	10.0	10.1	9.9	9.4	10.7
S (ppm)	1120	91	947	493	57	24	1030	24	245	1000	269	33
Cr	334	267	284	307	383	334	303	253	402	355	370	396
Ni	104	86	93	172	143	142	97	94	111	121	135	136
Cu	90	35	84	20	43	20	87	20	77	89	81	16
Zn	69	44	72	45	39	40	62	32	35	63	44	42
Ga	15	15	15	14	14	15	15	15	14	14	14	13
Sr	56	58	55	62	66	81	55	54	77	57	53	52
Y	26	30	26	25	29	30	25	29	27	23	25	24
Zr	44	54	50	58	64	64	47	55	58	42	42	40
FM	49.7	54.3	53.3	46.6	46.1	47.0	52.3	50.9	50.3	49.4	48.0	50.6
Mg#	0.64	0.60	0.61	0.67	0.68	0.67	0.62	0.63	0.64	0.65	0.66	0.63
Ox	21.4	21.1	25.6	20.7	22.5	24.6	29.0	22.0	24.2	22.4	18.7	18.3
Y/Zr	0.59	0.56	0.52	0.43	0.45	0.47	0.53	0.53	0.47	0.55	0.60	0.60
Zr/TiO_2	0.0052	0.0051	0.0052	0.0061	0.0063	0.0062	0.0052	0.0053	0.0060	0.0051	0.0051	0.0052

Table 1 (continued).

Leg:	140	140	140	140	140	140	140	140	140	140	140	140	140
Core-section:	226 R03	227 R01	227 R01	229 R01	230 R01	231 R01	233 R01	235 R01	235 R01	236 R01	237 R01	238 R01	238 R01
Interval (cm):	30–34	40–46	67–70	31–33	11–14	0–3	16–18	21–24A	21–24B	26–28	17–19	4–7	8–9
Piece no.:	3	7	8B	10	3	1	5	7	7	5	5	2	3
Depth (mbsf):	1923.2	1924.9	1925.2	1943.8	1953.1	1953.5	1960.1	1976.3	1976.3	1981.0	1983.9	1992.0	1992.0
Lithologic unit*:	260	260	260	265	265	265	266	269	269	269	269	269	269
Unit rock name:	mCOPD	mCOPD	mCOPD	sPOCD	sPOCD	sPOCD	AD	mPOCD	mPOCD	mPOCD	mPOCD	mPOCD	mPOCD
Alteration (%):	20		60	50	40	55	60	20	45	60	20	25	25
Alteration type:	D	D	P	L	L	L	L	D	H	P	D	D	D
SiO_2 (wt%)	46.5	48.5	49.0	49.5	50.5	51.0	50.0	49.4	49.7	49.2	48.5	50.1	49.7
TiO_2	0.86	0.67	0.54	0.90	1.06	0.90	0.94	0.84	0.81	0.64	0.84	0.90	0.69
Al_2O_3	16.5	16.6	16.4	15.0	14.6	14.7	14.6	16.4	16.0	16.7	16.1	15.3	15.8
Fe_2O_3	2.54	n.d.	1.98	1.80	2.59	2.19	2.15	2.23	2.27	1.91	2.68	2.90	2.10
FeO	6.71	n.d.	6.95	6.75	7.66	7.84	7.15	6.27	6.87	6.29	6.23	6.39	6.57
MnO	0.16	0.15	0.16	0.16	0.17	0.15	0.16	0.15	0.15	0.13	0.16	0.17	0.15
MgO	8.95	8.97	9.69	8.60	8.28	8.34	8.50	8.71	8.68	9.30	8.83	9.14	9.17
CaO	12.8	12.9	12.7	13.3	12.5	12.5	12.7	13.3	13.3	12.9	13.4	13.2	13.2
Na_2O	1.73	1.69	1.55	1.72	2.08	1.92	1.97	1.84	1.84	1.73	1.83	1.82	1.81
P_2O_5	0.07	0.06	0.05	0.06	0.08	0.07	0.07	0.07	0.06	0.05	0.06	0.07	0.05
H_2O^+	1.91	1.55	2.09	1.20	1.07	1.38	1.25	1.33	1.50	1.90	1.23	1.01	1.60
Sum	98.7	100.1	101.1	99.0	100.6	101.0	99.5	100.5	101.2	100.8	99.9	101.0	100.8
Fe_2O_{3T}	10.0	9.0	9.7	9.3	11.1	10.9	10.1	9.2	9.9	8.9	9.6	10.0	9.4
S (ppm)	479	n.d.	952	60	179	20	125	741	99	6	847	695	111
Cr	309	361	384	424	166	213	294	341	372	441	335	352	384
Ni	145	139	151	102	82	84	91	114	110	147	110	109	116
Cu	137	38	9	8	58	6	47	111	29	6	128	105	22
Zn	46	44	48	32	39	36	39	45	44	41	43	49	40
Ga	14	14	14	14	15	15	14	14	15	13	14	14	14
Sr	55	55	54	55	52	48	54	57	61	58	60	60	57
Y	23	21	17	26	29	28	28	24	24	18	23	24	21
Zr	45	34	28	48	52	44	49	43	46	34	44	48	36
FM	50.1	47.4	47.4	49.3	54.7	54.0	51.7	48.7	50.6	46.3	49.5	49.6	48.0
Mg#	0.64	0.69	0.66	0.65	0.60	0.60	0.63	0.65	0.63	0.67	0.65	0.64	0.66
Ox	25.4		20.4	19.3	23.3	20.1	21.3	24.3	22.9	21.5	27.9	29.0	22.3
Y/Zr	0.51	0.62	0.61	0.54	0.56	0.64	0.57	0.56	0.52	0.53	0.52	0.50	0.58
Zr/TiO_2	0.0052	0.0051	0.0052	0.0053	0.0049	0.0049	0.0052	0.0051	0.0057	0.0053	0.0052	0.0053	0.0052

Table 2. Rare earth element (REE) abundances of selected Leg 137/140 diabase samples.

Leg:	137	137	140	140	140	140	140	140	140	140	140	140	140	140	140
Core-section:	177 R01	186 R02	187 R01	187 R01	189 R01	189 R01	189 R01	189 R02	193 R01	193 R01	193 R01	194 R01	196 R01	197 R01	198 R01
Interval (cm):	48–51	30–36	59–63A	59–63B	85–88	90–94A	90–94B	15–17	28–31	44–46	58–60	42–46	21–26	29–31	50–54
Piece no.:	13	8	14	14	19	20	20	3	9	13A	14	8	4	7	14
Alteration type:	D	L	D	P	D	D	H	P	P	H	P	P	D	H	D
La	1.0	1.5	0.9	0.8	1.0	0.9	0.7	0.60	0.7	1.0	0.5	0.5	1.4	0.8	0.9
Ce	5.0	6.8	4.4	4.1	5.0	4.7	3.3	3.0	2.2	4.9	2.6	2.4	5.4	3.8	4.3
Nd	4.7	5.5	4.0	3.5	4.6	4.6	3.3	2.8	2.0	4.4	2.2	2.4	4.5	3.6	3.9
Sm	2.1	2.1	1.8	1.6	2.0	2.1	1.6	1.3	0.7	2.1	1.5	1.2	1.8	1.3	1.5
Eu	0.83	0.82	0.79	0.84	0.77	0.80	0.65	0.57	0.42	0.73	0.74	0.55	0.78	0.72	0.71
Gd	3.4	3.4	3.2	2.7	3.4	3.3	2.3	2.2	1.6	3.0	1.8	1.8	3.0	2.7	3.0
Dy	4.7	4.6	4.4	3.8	4.5	4.5	3.4	3.0	2.2	4.4	2.5	2.5	4.4	3.7	3.9
Ho	0.99	0.94	0.93	0.80	0.95	0.95	0.69	0.65	0.43	0.90	0.47	0.51	0.94	0.75	0.79
Er	3.1	2.9	2.8	2.5	2.9	3.0	2.2	1.9	1.4	2.8	1.5	1.5	2.8	2.3	2.6
Yb	2.9	2.8	2.7	2.4	2.8	2.9	2.2	2.0	1.3	2.6	1.6	1.6	2.7	2.2	2.4
Lu	0.46	0.44	0.42	0.38	0.44	0.46	0.34	0.30	0.21	0.38	0.23	0.24	0.42	0.34	0.38
Sum REE	29.0	31.8	26.3	23.4	28.3	28.2	20.7	18.3	13.1	27.2	15.6	15.2	28.1	22.2	24.4
La/Sm	0.48	0.71	0.50	0.50	0.51	0.44	0.45	0.46	0.97	0.48	0.33	0.38	0.78	0.61	0.61

Table 2 (continued).

Leg:	140	140	140	140	140	140	140	140	140	140	140	140	140	140	140
Core-section:	199 R01	200 R02	202 R01	204 R01	207 R01	208 R03	209 R01	209 R01	209 R01	209 R02	211 R01	213 R01	214 R01	214 R01	214 R01
Interval (cm):	54–57	53–57	23–25	15–19	22–26	7–10	35–41A	35–41B	98–102	68–70	70–74	64–68	24–28	36–40	73–76
Piece no.:	13	7B	7	4	6	1	6A	6A	14	10	16	19	5A	5	8
Alteration type:	D	D	H	L	D	P	D	P	P	D	D	D	P	D	P
La	1.0	0.9	0.9	1.2	1.2	0.7	0.9	0.7	0.4	1.1	0.9	0.9	0.7	0.8	0.5
Ce	4.4	4.2	4.4	6.3	5.2	3.5	4.4	3.0	2.0	4.4	4.1	4.1	3.3	3.4	2.3
Nd	3.7	3.6	3.8	5.1	4.7	2.9	4.0	2.7	2.1	3.6	3.9	3.4	2.6	3.0	2.2
Sm	1.5	1.4	1.6	1.9	2.0	1.4	1.7	1.2	1.1	1.6	1.8	1.4	1.3	1.4	1.0
Eu	0.69	0.67	0.73	0.92	0.88	0.58	0.64	0.57	0.69	0.62	0.73	0.69	0.60	0.67	0.66
Gd	2.4	2.5	2.8	3.3	3.2	2.0	2.5	2.1	1.6	2.7	3.1	2.6	2.0	2.5	1.6
Dy	3.5	3.4	4.0	4.3	4.6	2.6	3.5	2.6	2.1	3.3	4.0	3.7	2.8	3.2	2.2
Ho	0.73	0.71	0.86	0.88	0.95	0.55	0.74	0.53	0.43	0.68	0.84	0.77	0.57	0.67	0.40
Er	2.1	2.1	2.6	2.7	2.9	1.7	2.3	1.6	1.3	2.1	2.6	2.3	1.8	2.1	1.4
Yb	2.1	1.9	2.5	2.6	2.8	1.6	2.2	1.6	1.3	2.0	2.6	2.3	1.8	2.0	1.4
Lu	0.30	0.31	0.40	0.39	0.44	0.26	0.34	0.25	0.19	0.32	0.40	0.35	0.27	0.31	0.20
Sum REE	22.4	21.7	24.6	29.6	28.9	17.8	23.2	16.8	13.2	22.4	25.0	22.5	17.7	20.1	13.8
La/Sm	0.67	0.65	0.56	0.63	0.60	0.50	0.50	0.55	0.36	0.69	0.50	0.64	0.54	0.57	0.48

Table 2 (continued).

Leg	140	140	140	140	140	140	140	140	140	140	140	140	140	137
Core-section:	216 R01	220 R01	222 R01	222 R01	222 R01	224 R01	225 R02	225 R02	225 R02	230 R01	235 R01	235 R01	238 R01	182 M03
Interval (cm):	54–56	23–26	69–73	115–120A	115–120B	38–42	29–32	68–72A	68–72B	11–14	21—24A	21–24B	4–7	7–20
Piece no.:	12	6	12A	12	22	8	5	13	13	3	7	7	2	BAS 140
Alteration type:	D	D	D	D	P	D	D	D	H	L	D	H		
La	1.0	1.1	1.4	1.5	1.3	1.2	1.4	0.9	0.8	1.1	1.0	0.9	1.1	1.0
Ce	4.5	5.4	6.2	6.3	6.4	4.7	5.3	3.9	4.1	5.3	4.6	4.2	4.5	4.8
Nd	4.0	4.4	4.8	5.4	5.4	4.2	4.2	3.8	3.7	4.6	4.0	3.6	4.2	4.5
Sm	1.4	1.8	1.9	2.2	2.1	1.7	1.5	1.6	1.5	1.9	1.9	1.7	1.7	2.0
Eu	0.72	0.86	0.74	0.82	0.83	0.78	0.73	0.69	0.84	0.80	0.74	0.83	0.78	0.61
Gd	2.9	3.1	3.1	3.3	3.4	2.9	2.8	2.7	2.9	3.4	2.9	2.7	2.9	3.1
Dy	4.0	4.5	4.2	4.6	4.6	4.0	3.9	3.8	3.6	4.6	4.0	3.7	4.0	3.5
Ho	0.83	0.95	0.89	0.99	0.97	0.84	0.84	0.79	0.76	0.96	0.82	0.78	0.84	0.87
Er	2.5	2.8	2.7	3.0	2.9	2.5	2.5	2.4	2.3	3.0	2.5	2.3	2.5	2.6
Yb	2.4	2.7	2.6	2.8	2.8	2.4	2.4	2.4	2.4	2.8	2.4	2.2	2.4	2.5
Lu	0.37	0.43	0.41	0.45	0.45	0.39	0.38	0.38	0.38	0.44	0.37	0.34	0.39	0.40
Sum REE	24.6	28.0	28.9	31.4	31.2	25.6	26.0	23.4	23.3	28.9	25.2	23.3	25.3	25.7
La/Sm	0.68	0.61	0.74	0.68	0.62	0.71	0.93	0.59	0.53	0.58	0.53	0.53	0.65	0.51

Notes: Alteration type: D = macroscopically dark, less altered diabase; L = macroscopically light, high background alteration; H = diabase containing high percentage of halos around veins; P = samples with green patches or vugs and a high background alteration.

Table 3. Major and trace element data for an international reference rock BHVO-1, an interlaboratory standard Bas 140, and a comparision between shipboard and laboratory data.

	BHVO-1			Bas 140			209R-1, 98–102 cm	
	This study	2s std. dev.	Govindaraju (1989)	This study	2s std. dev.	Shipboard report*	This study	Shipboard report*
SiO_2 (wt%)	50.01	0.15	49.9	50.6	0.46	50.59	48.6	49.34
TiO_2	2.76	0.04	2.71	1.00	0.02	0.97	0.42	0.39
Al_2O_3	13.80	0.06	13.8	14.6	0.26	14.59	15.9	15.99
Fe_2O_3 total	12.53	0.09	12.2	11.3	0.14	11.16	11.2	11.15
MnO	0.17	0.01	0.17	0.19	0.02	0.18	0.16	0.16
MgO	7.31	0.04	7.23	8.21	0.10	8.02	9.23	9.22
CaO	11.51	0.06	11.4	12.5	0.08	12.51	11.4	11.54
Na_2O	2.28	0.02	2.26	1.78	0.04	1.84	1.61	1.82
K_2O	0.52	0.01	0.52	n.d.	n.d.	0.003	n.d.	0.0024
P_2O_5	0.28	0.01	0.27	0.08	0.02	0.06	0.03	0.01
H_2O^+	n.d.	n.d.	n.d.	1.15	0.05	1.25	3.15	3.00
Cr (ppm)	299	10	289	194	4	175	413	418
Ni	114	2	121	81	3	84.1	128	134.5
Cu	143	4	136	83	4	82.6	9	13.1
Zn	103	2	105	78	2	75.8	65	60.7
Ga	21	2	21	16	2	n.d.	12.6	n.d.
Rb	11	1	11	<5	n.d.	<0.4	<5	<0.4
Sr	400	5	403	47	2	44.5	50	51.7
Y	26	2	28	27	2	25.9	12	11.0
Zr	172	3	179	49	1	45.4	25	19.4
Nb	19	1	19	<5	n.d.	0.5	<5	<0.3

Notes: n.d. = not determined; std. dev. = standard deviation.
*Shipboard Scientific Party (1992).

Table 4. Reference data for the determination of Fe^{2+}, S, and H_2O.

Sample	Element	This study	2s std. dev.	Govindaraju (1989)	Lab data
MRG-1	S	310	26	313	
GXR-2	S	644	40	610	
Andesite	Fe^{2+}	6.23	0.12		6.28
MRG-1	H_2O^+	1.05	0.08	1.03	
BE-N	H_2O^+	2.25	0.07	2.24	

Note: std. dev. = standard deviation.

Table 5. Modal compositions of selected Leg 137/140 diabase samples by XRD analysis.

Leg:	137	137	140	140	140	140	140	140	140	140	140	140	140	140	140	140
Core-section:	173 R01	186 R02	187 R01	187 R01	189 R01	190 R01	194 R01	196 R01	197 R01	198 R01	199 R01	200 R02	202 R01	204 R01	207 R01	209 R01
Interval (cm):	73–76	30–32	59–63A	59–63B	85–88	10–14	36–40	21–26	29–31	50–54	54–57	53–57	23–25	15–19	22–26	98–102
Piece no.:	9	8	14	14	19	2	7	4	7	14	13	7B	7	4	6	14
Depth (mbsf):	1570.7	1628.1	1632.6	1632.6	1651.9	1655.2	1680.8	1696.7	1703.1	1712.7	1719.9	1730.6	1747.4	1756.7	1768.6	1788.5
Lithologic unit:*	193	213	216	216	218	218	220	222	222	223	226	227	229	232	236	240
Unit rock name:	OPC	AD	sPCD	sPCD	mPOCD	mPOCD	mPOCD	mPOCD	mPOCD	sPOCD	mPOCD	mPOCD	sPOCD	sPCOD	AD	mOPCD
Alteration (%):	40	35	25	90	12	60	20	15	70	20	15	10	25	45	40	78
Alteration type:	L	L	D	P	D	P	D	D	H	D	D	D	H	L	D	P
%																
Plagioclase	49	42	48	30	45	33	42	45	48	48	53	53	44	46	43	34
Amphibole	15	14	16	53	11	37	12	13	28	0	0	0	10	18	35	0
Chlorite	10	14	2	5	3	13	3	3	11	7	4	2	4	6	0	19
Clinopyroxene	27	30	33	12	37	16	42	35	13	39	38	41	41	30	22	46
Quartz	0	0	0	0	4	0	2	4	0	0	0	0	0	0	0	0
Talc	0	2	0	0	2	0	0	0	0	6	5	3	0	0	0	0
Sum	101	102	99	100	102	99	101	100	100	100	100	99	99	100	100	99

Notes: Unit rock name: m = moderately; s = sparsely; O = olivine; P = plagioclase; C = clinopyroxene; D = diabase; A = aphyric. Alteration type: D = macroscopically dark, less altered diabase; L = macroscopically light, high background alteration; H = diabase containing high percentage of halos around veins; P = samples with green patches or vugs and a high background alteration. *Shipboard Scientific Party (1992).

Table 5 (continued).

Leg:	140	140	140	140	140	140	140	140	140	140	140	140	140	140	140
Core-section:	209 R02	211 R01	213 R01	214 R01	216 R01	220 R01	222 R01	222 R01	222 R01	224 R01	225 R02	230 R01	235 R01	235 R01	238 R01
Interval (cm):	68–70	70–74	64–68	36–40	54–56	23–26	69–73	115–120A	115–120B	38–42	29–32	11–14	21–24A	21–24B	4–7
Piece no.:	10	16	19	5	12	6	12A	12	22	8	5	3	7	7	2
Depth (mbsf):	1789.6	1799.2	1813.1	1819.0	1828.4	1865.7	1885.3	1885.8	1885.8	1904.1	1914.0	1953.1	1976.3	1976.3	1992.0
Lithologic unit:*	240	241	243	244	245	252	254	256	256	258	260	265	269	269	269
Unit rock name:	mOPCD	sPOCD	sPOCD	mPOCD	mCOPD	mCOPD	mCOPD	AD	AD	mCPOD	mCOPD	sPOCD	mPOCD	mPOCD	mPOCD
Alteration (%):	15	30	35	50	15	10	45	45	70	8	15	40	20	45	25
Alteration type:	D	D	D	D	D	D	D	D	P	D	D	L	D	H	D
%															
Plagioclase	51	47	45	44	42	40	48	33	36	39	49	38	50	40	44
Amphibole	0	0	10	13	0	0	0	19	32	0	0	62	12	39	11
Chlorite	4	6	9	8	9	4	14	12	7	2	3	0	2	2	4
Clinopyroxene	41	47	36	35	49	49	38	36	26	55	48	0	35	19	42
Quartz	0	0	0	0	0	5	0	0	0	0	0	0	0	0	0
Talc	4	1	0	0	0	0	0	0	0	4	1	1	0	0	1
Sum	100	101	100	100	100	98	100	100	101	100	101	101	99	100	102